Advances in Science and Technology Research Journal, 2025, 19(12), 138–155 https://doi.org/10.12913/22998624/209886 ISSN 2299-8624, License CC-BY 4.0

# Structural and dynamic performance of a street sweeper chassis with diagonal suspension subjected to standard speed bumps

Christian David Silva Guzman<sup>1</sup>, Edwin Efrain Condori Jacinto<sup>1</sup>, Yuri Lester Silva Vidal<sup>1</sup>, Waygand Freddy Beltran Quispe<sup>1</sup>, Christofer Alex Diaz Arapa<sup>1</sup>

- <sup>1</sup> Department of Mechanical Engineering, Universidad Nacional de San Agustín de Arequipa, Santa Catalina 117, Arequipa 04000, Peru
- \* Corresponding author's e-mail: wbeltrang@unsa.edu.pe

#### **ABSTRACT**

This study presents the design and validation of a chassis made from AISI 1040 steel for unmanned electric street sweepers, focusing on its structural response to standard road humps in urban environments. Finite element analysis (FEA) was conducted in Altair Inspire, and dynamic simulations were performed in MATLAB Simulink to evaluate both static and regulatory dynamic loads, including speed bump impacts. A diagonal suspension system was integrated to improve load distribution, reducing deformations by 22% compared to conventional configurations. Modal analysis revealed three critical vibration modes (50.33 Hz, 69.85 Hz, and 78.11 Hz), each with effective mass participation above 15%, informing structural reinforcements. Dynamic simulations confirmed that the proposed chassis design maintains high structural integrity under transient urban loading scenarios, with stress levels significantly below the elastic limit of AISI 1040 steel. Leveraging meshless finite element analysis and quarter-car dynamics, the structure proved resilient to road-induced impacts, ensuring durability, minimal deformation, and adaptability.

Keywords: vehicle chassis, modal analysis, dynamic load simulation, AISI 1040 steel, structural analysis.

#### **INTRODUCTION**

The structural analysis of unmanned vehicle chassis must address both static and dynamic performance to ensure the operational integrity of critical components such as motors and batteries [1]. These dual demands arise from the necessity to support the permanent weight of onboard systems while simultaneously absorbing transient loads caused by irregular urban terrain [2, 3].

In this context, AISI 1040 steel tubing offers an excellent balance of machinability and weldability, enabling the fabrication of complex geometries [4]. Its notable mechanical resilience, especially impact resistance, makes it particularly suitable for unmanned electric vehicles operating in demanding environments[5]. Our finite element analysis (FEA) methodology [6] is applied

to identify critical stress concentrations and validate the chassis's load-bearing capacity without compromising component safety, similar to methodologies in earlier works [7].

Received: 2025.07.28

Accepted: 2025.10.01

Published: 2025.11.01

This integrated approach enhances structural robustness while ensuring protection against environmental and operational stresses [8]. The design specifically addresses the urban topography of cities like Arequipa, Peru, characterized by fragmented pavements, speed bumps, and steep gradients [9]. These conditions require advanced design strategies for vibration damping and fatigue resistance [2, 10], particularly under repetitive impacts such as potholes [6]. Therefore, the chassis must effectively balance multidirectional load absorption with long-term structural durability.

The future of urban services lies in automation. In this context, the design of unmanned vehicles for tasks such as street sweeping presents unique challenges, especially in complex and variable topographies like those of Arequipa, Peru. The structural resilience of these vehicles is fundamental to ensuring their long-term reliability, as they must withstand both the constant weight of their components and the dynamic loads generated by speed bumps, potholes, and irregular pavements. A robust design approach and an exhaustive analysis are essential to ensure that the chassis of the unmanned electric sweeper not only fulfills its purpose but also effectively protects internal systems and minimizes maintenance costs throughout its service life.

To address these challenges, this study focuses on the dynamic response of the chassis under transient loads, a facet that is underexplored in lightweight vehicles with unconventional suspension configurations. The implementation of a diagonal suspension is a critical aspect of our design, as it directly influences load distribution and impact absorption capacity. To evaluate its performance realistically, we use a quarter-car model in MATLAB Simulink, complemented by a geometric correction function that accurately translates vertical displacement into the actual compression of the shock absorber.

The objective of this research is twofold: (1) To quantify the dynamic forces acting on the chassis and (2) To validate a hybrid methodology that combines system dynamics with meshless finite element analysis. Specifically, our approach will allow us to determine the factor of safety under both static and dynamic conditions, enabling an exhaustive comparison that confirms the suitability of the AISI 1040 material and validates the structural integrity of the design against the challenges of the urban environment.

#### **METHODOLOGY**

The structural analysis of the chassis was performed using a multilevel simulation framework that integrates dynamic system modeling with advanced finite element analysis. This approach was specifically chosen to provide a realistic assessment of the chassis's response to the challenging urban environment of Arequipa, where static and dynamic loads coexist.

To model the dynamic forces induced by irregular terrain, a quarter-car mathematical model

was implemented in MATLAB/Simulink. This model captured the vertical interaction between the chassis and road irregularities, such as speed bumps and fragmented surfaces [11]. A key feature of this model was the inclusion of a geometric correction function to account for the diagonally oriented suspension system, which is essential for accurately translating vertical displacement into the actual shock absorber compression force. This step ensured the dynamic loads applied to the chassis were physically representative of the vehicle's unique design.

The analysis was divided into three main stages to provide a comprehensive evaluation of the chassis's structural integrity. First, a static analysis was performed in Altair SimSolid<sup>TM</sup> to establish a baseline response, evaluating stress distribution and deformation under the fixed gravitational load of the vehicle's components and a full garbage load. Second, the dynamic forces from the Simulink model were used as inputs for a transient structural analysis. This stage allowed for the prediction of peak von Mises stresses and displacements under realistic impact scenarios, confirming the chassis's resilience under short-duration, high-magnitude loads. Finally, a modal analysis was conducted to determine the natural frequencies and critical vibration modes of the structure. This step was crucial for identifying potential resonance risks and evaluating the overall dynamic stiffness of the chassis.

The use of this meshless finite element technology [12] was a strategic choice, as it allowed for the efficient simulation of the chassis's complex geometry without the time-consuming preprocessing and numerical issues associated with traditional meshing. This methodology enabled us to perform a comprehensive evaluation of both static and dynamic performance, including stress distribution, deformation, and critical vibration modes. By combining these advanced simulation tools, we established a robust foundation for design validation, ensuring the chassis's durability and integrity under the demanding scenarios of its target operational environment.

#### Vehicle description

The vehicle features a compact design, measuring 1.2 meters in length, 0.7 meters in width, and 480 mm in height from the ground. Its chassis incorporates a mobile platform inspired by ATV-style suspension systems, enabling terrain adaptation during movement.

The collection process begins with circular brushes that guide waste toward the vehicle's center. The access ramp includes a flexible flap that lifts upon contact with larger objects, allowing their entry. Subsequently, a cylindrical brush pushes the debris into the storage compartment, which has a capacity of 290 mm in length, 250 mm in height, and 700 mm in width. To improve stability, the suspension system is arranged diagonally, seeking optimal center of gravity balance. The chassis is constructed from 2 mm thick steel sheet, with main longitudinal members of 30 mm diameter and secondary reinforcements of 20 mm diameter, providing structural strength.

Table 1 summarizes the technical specifications of the main vehicle components, organized into four key systems: propulsion, cleaning (circular and cylindrical brushes), and energy storage. It details dimensions, mass, and relevant power/torque parameters for structural and dynamic analysis of the assembly. The N/A values indicate passive components or non-driving elements, which will mainly serve for static analysis.

Figures 1 and 2 show the components and their respective positions in the vehicle, which will be used to define the position of various loads in subsequent analyses.

#### Static structural analysis

The structural analysis of the chassis was conducted using finite element analysis (FEA) in SolidWorks and Altair Inspire. AISI 1040 steel tubing was selected for its manufacturability, particularly in rolled joints to minimize welds and stress concentrations [13]. The 3D model was optimized for static and dynamic loads and exported to Altair Inspire for deformation zone analysis under distributed and point loads simulating operational conditions. Boundary conditions were fixed at suspension supports. Stress and deformation results were compared to the material's strength to validate safety margins in demanding environments [14, 15].

To evaluate the structural performance of the chassis under stationary loading, a static analysis was performed in Altair SimSolid. A gravity load of approximately 1298.9 N was applied, corresponding to the combined mass of the onboard components (82.4 kg) and a full 50 kg garbage load. This force was applied in the vertical direction with fixed supports defined at the wheel positions. The objective was to establish a baseline response prior to transient dynamics.

The maximum von Mises stress obtained was 1.68 MPa, significantly lower than the yield strength of AISI 1040 steel (353 MPa), confirming that the

Table 1. Detail of the components of the unmanned cleaning vehicle and its main characteristics

	Motion S	ystem					
Equipment	Dimensions (mm)	Mass (kg)	Power/Torque				
Main Chassis	Main Chassis L:1200, a:700, h:480		N/A				
Traction Motor	Ø180 x 220	7	2.2 kW / 70 Nm				
Wheels (4)	Ø200 x 50	2	N/A				
Shock Absorbers (4)	Center a center: 212	3	N/A				
	Cleaning System, 0	Circular Brushes					
Equipment	Dimensions (mm)	Mass (kg)	Power/Torque				
Brush Motor	Brush Motor Ø80-100		400W / 0.7 Nm				
Transmission Variable		2	N/A				
	Cleaning System, Cylindrical Brush						
Equipment	Equipment Dimensions Mass (kg) Power/Torqu						
Brush motor	Ø150 x 200	6	300W / 1.5 Nm				
Brush cylinder	Brush cylinder Ø450 x 300		N/A				
	Energy Storage System						
Equipment	Dimensions (mm)	Mass (kg)	Power/Torque				
Batteries	250 x 170 x 150	14/Unidad	48V, 50Ah				

**Note:** Specifications are grouped by system to facilitate structural and dynamic analysis. N/A indicates passive or non-driving components.

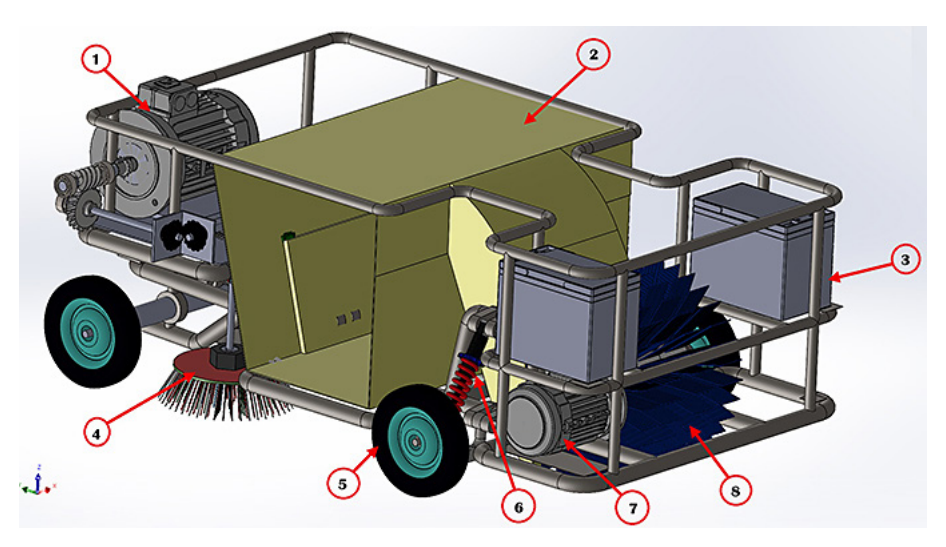


**Figure 1.** Isometric view of the cleaning vehicle showing: (1) Circular brush motor, (2) Waste storage compartment, (3) Batteries, (4) Circular brush, (5) Wheel (8 inches), (6) Shock absorber, (7) Cylindrical brush motor, (8) Cylindrical brush

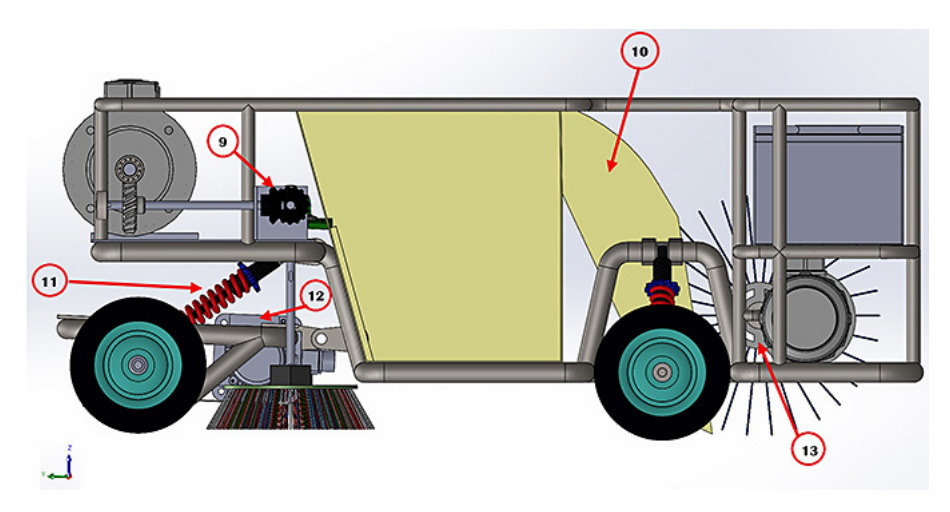


**Figure 2.** Additional view of the cleaning vehicle showing: (9) Circular brush transmission system, (10) Waste storage intake, (11) Rear shock absorber, (12) Traction motor, (13) Cylindrical brush drum

structure remains well within the elastic range. The maximum displacement observed was 0.21 mm, occurring in the upper central region of the roof, which is far from the load-bearing zones. This validates the structural stiffness and design integrity of the chassis for quasi-static operating conditions.

#### Dynamic analysis

Dynamic analysis of the chassis is essential to understand its behavior under variable loads and impact events in real-world environments, such as Arequipa's uneven roads. Techniques like modal analysis and transient analysis help identify the system's natural frequencies and evaluate its response to short-duration, high-magnitude

forces that may cause concentrated stresses or excessive deformations. Prior studies [6, 16] demonstrate that accurate identification of natural frequencies is key to avoiding resonance that could compromise structural integrity. However, research [17] warns that omitting additional weights from accessories, occupants, or internal components may underestimate actual stresses and reduce analysis accuracy.

In this case, transient analysis through timedependent load simulations such as impact forces from obstacles or potholes is critical to verify the chassis's energy dissipation capacity and structural resilience under rapid loading events. Evidence from similar studies [6,16] confirms that simulated impact loads via sinusoidal functions or acceleration data can validate design safety, showing peak stresses within allowable limits and sufficient safety factors to withstand abrupt events on rough terrain. Evaluating these loads in the FEM model ensures the vehicle is not only safe for daily operation but also resilient enough to endure environmental challenges, protecting internal components and extending system lifespan.

#### Advanced finite element modeling

Finite element analysis (FEA) is crucial for validating the structural performance of unmanned vehicle chassis, though it often suffers from stress singularities unrealistic concentrations that distort results, especially at sharp edges [18, 19]. These are worsened by complex geometries and coarse meshes, which demand timeconsuming refinements or simplifications [12, 20]. To overcome this, Altair SimSolid™ offers a meshless alternative based on external approximation theory, enabling accurate analysis without preprocessing, ideal for irregular urban terrains like Arequipa's [9]. In this work, SimSolid was applied for static and transient analysis under realistic load scenarios. A modal analysis determined the system's natural frequencies [6, 17], while dynamic loads from MATLAB Simulink simulations of obstacle impacts enabled stress and deformation predictions, supporting the derivation of a dynamic load factor for improved design. To deepen the dynamic response assessment, a quarter-car mathematical model was implemented. This model captures the vertical interaction between the chassis and road irregularities such as potholes and uneven surfaces, providing a simplified yet effective framework to analyze suspension behavior [21]. The system was modeled with two degrees of freedom: the sprung mass (ms), representing part of the chassis structure, and the unsprung mass (mu), associated with the wheels and suspension components (Figure 3).

Key mechanical parameters include the suspension stiffness (ks), damping coefficient (cs), and tire vertical stiffness (kt). Damping from tires was neglected, given its relatively low magnitude compared to that of the suspension system [21]. In this application, the chassis utilizes a diagonally oriented suspension adapted to urban scenarios, which modifies stress distribution during dynamic events and enhances impact absorption.

External terrain-induced forces were modeled through displacement functions  $z_r(t)$  representing

typical obstacle profiles encountered in Arequipa. Newtonian equations of motion were used to calculate the vertical responses  $z_s(t)$  and  $z_u(t)$  of the suspended and unsuspended masses, respectively. Particular attention was given to the compression phase of the shock absorber, which is critical for transmitting peak loads to the chassis structure [22]. The damping coefficients used in this phase were selected from manufacturer data and adjusted for various terrain conditions, slopes, and vehicle speeds.

This multilevel simulation framework, which combines meshless finite element analysis with dynamic system modeling, ensures that the designed chassis can effectively withstand structural fatigue and deformation, thereby protecting internal components and extending the vehicle's service life in harsh urban environments.

## DYNAMIC FUNDAMENTALS OF THE QUARTER-VEHICLE MODEL

Using Newton's second law of motion, the differential equations governing the system's dynamic behavior were established (from Equation 1–7). For the suspended mass (chassis), the force balance is expressed as [6]:

For the suspended mass:

$$\Sigma F = ma \tag{1}$$

$$m_s(\ddot{z}_s - g) = f_{susp} - f_g \tag{2}$$

where: g – gravitational constant,  $f_{susp}$  – suspension force transmitted to the chassis,  $f_g$  – static load due to gravity =  $m_s g$ .

The gravitational force and acceleration are constant variables that can be simplified in the equation, allowing their elimination to facilitate analysis:

$$m_s \ddot{z}_s = f_{susp} \tag{3}$$

Thus, the force transferred to the chassis at the suspension point is obtained directly by:

$$f_{susp} = k_s (z_u - z_s) + c_s (\dot{z}_u - \dot{z}_s)$$
(4)

By integrating Equations 3 and 4:

$$m_{s}\ddot{z}_{s} = f_{susp} = k_{s}(z_{u} - z_{s}) - c_{s}(\dot{z}_{u} - \dot{z}_{s})$$
 (5)

For the unsprung mass:

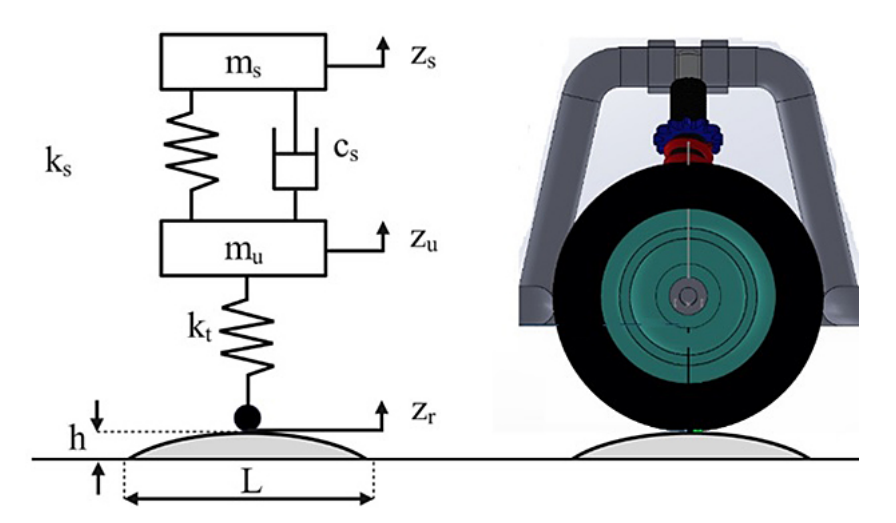


Figure 3. Simplified representation of the suspension system

$$m_u \ddot{z}_u = k_t (z_r - z_u) - -k_s (z_u - z_s) - c_s (\dot{z}_u - \dot{z}_s)$$
 (6)

The free-body diagram in Figure 4 illustrates the forces acting on the chassis, including impacts, suspension, and weight. Equations 5 and 6 represent the motion laws, modeled in MATLAB Simulink (Figure 5). This enables simulation of the response to rapid loads and deformations caused by irregular terrain, ensuring structural resistance under extreme conditions.

Table 2 shows the mechanical properties of AISI 1040 steel used as input parameters for the structural and dynamic analyses. The strength values and elastic moduli were verified against

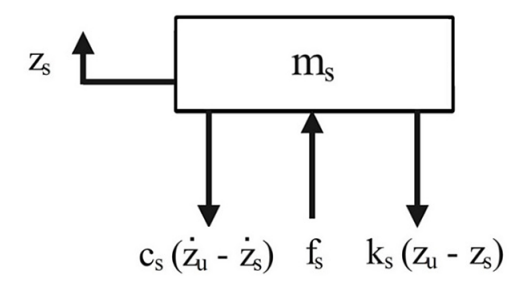


Figure 4. Free-body diagram of the suspended mass

**Table 2.** Properties of AISI 1040 steel [4]

Parameter	Value		
Yield strength	353 MPa		
Tensile strength	519 MPa		
Poisson's ratio	0.27-0.30		
Density	7.85 g/cm <sup>3</sup>		
Elastic modulus	190-210 GPa		
Shear modulus	80 GPa		

technical standards [4] to ensure simulation accuracy. Table 3 details the mechanical parameters adopted in the simplified quarter-car suspension model used for dynamic analysis.

The integration of the function to calculate the angular variation of the shock absorber in the simulation model is essential for an accurate representation of the chassis' dynamic behavior. In practice, the diagonal arrangement of the shock absorber means that a linear spring displacement (represented by measurement 'x') does not directly translate into identical chassis movement. To address this, the "calculate cos alpha" function models this critical geometric relationship and provides a more realistic simulation of the chassis' vertical motion, considering the shock absorber's working angles. As shown in Figure 6, this function takes two key inputs: zs (the vertical displacement of the sprung mass) and zu (the vertical displacement of the unsprung mass). The function then processes this data internally to output the cos alpha value, which is crucial for accurately translating the diagonal movement of the shock absorber into the effective vertical displacement. This is a fundamental step for capturing how forces and impacts are transmitted, ensuring the validity of dynamic

**Table 3.** Parameters of the simplified suspension system

Parameter	Value		
Suspended mass (m <sub>s</sub> )	50 kg		
Unsprung mass (m <sub>u</sub> )	8 kg		
Spring stiffness (k <sub>s</sub> )	8500 N/m		
Damping coefficient (c <sub>s</sub> )	3800 Ns/m		
Tire vertical stiffness (k <sub>t</sub> )	120000 N/m		

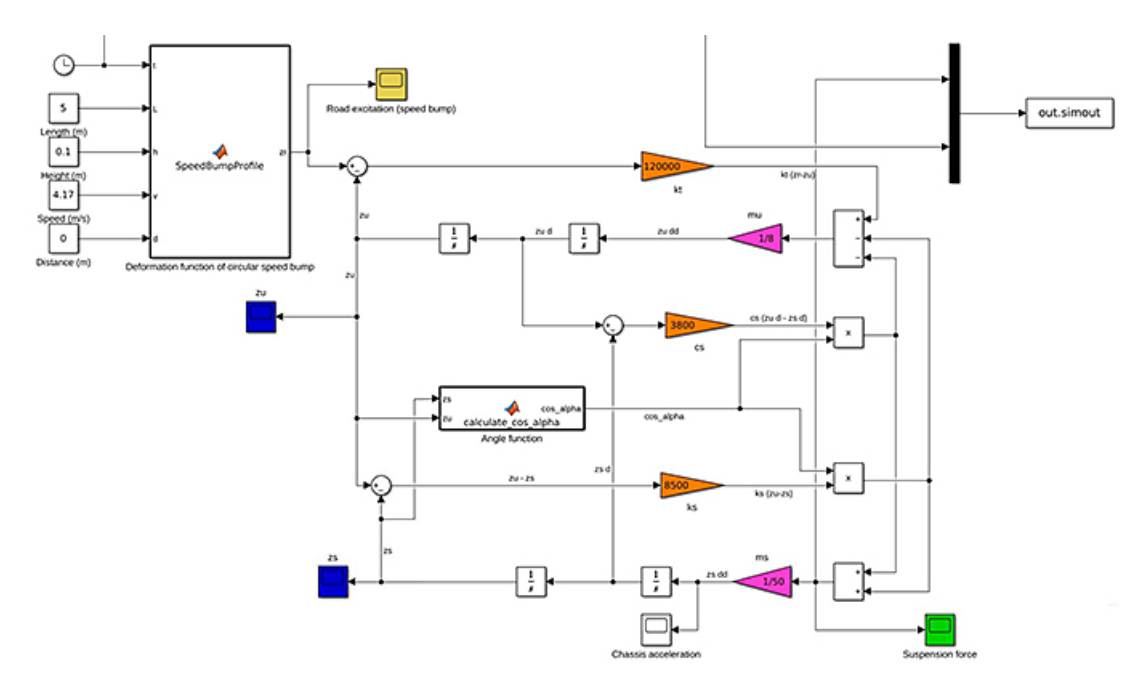


**Figure 5.** Simulink representation of the suspension system, with an integrated function to model the angle variation due to motion

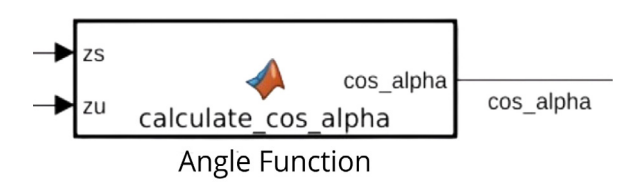


**Figure 6.** Schematic of the calculate\_cos\_alpha function in Simulink

analysis results and, ultimately, the effectiveness of the suspension system design.

The integration of a geometric correction function to calculate the angular variation of the shock absorber in the simulation model is essential for accurately representing the dynamic behavior of the chassis. In the diagonal configuration adopted, the vertical movement of the chassis does not correspond linearly with the compression of the shock absorber. This discrepancy is addressed through the implementation of the *calculate\_cos\_alpha* function, which corrects the vertical force component by dynamically computing the angle between the shock absorber and the vertical axis based on real-time displacement inputs.

This function receives as inputs the relative displacements of the sprung and unsprung masses (zs and zu), and computes the current orientation of the shock absorber with respect to the vertical (Z-axis). Using the nominal geometry specifically the initial shock absorber length ( $L_{shock\_nominal}$ ) and its inclination angle ( $\alpha_{nominal\_deg}$ ) the function

determines the nominal vertical and horizontal distances between the mounting points ( $V_{nominal}$  and  $L_{offset}$ ). During simulation, the current vertical offset ( $V_{current}$ ) is recalculated based on the dynamic displacement of the suspension system. The actual shock absorber length ( $L_{shock\_current}$ ) is derived via the Pythagorean theorem, and the cosine of the working angle ( $\cos \alpha$ ) is obtained as the ratio between  $V_{current}$  and  $L_{shock\_current}$ .

This angular correction is applied to modulate the suspension force vectors, thereby improving the physical fidelity of the quarter-vehicle model when encountering road irregularities such as potholes and speed reducers. Figure 6 illustrates the conceptual necessity of this function, while Figure 7 shows the Simulink block that generates the road excitation. As depicted, this block, named "SpeedBumpProfile", receives key inputs time (t), obstacle length (L), height (h), vehicle speed (v), and distance (d) which are adjusted for each simulation case, allowing for accurate and adaptable modeling of different speed bump profiles [23]. The function includes validation to ensure that the cosine value remains within the range [-1, 1], preventing numerical errors. In summary, this function links suspension component displacements with the system's geometry, accounting for the diagonal configuration of the shock absorber and providing an essential input for accurately modeling the forces acting on the chassis under dynamic road conditions.

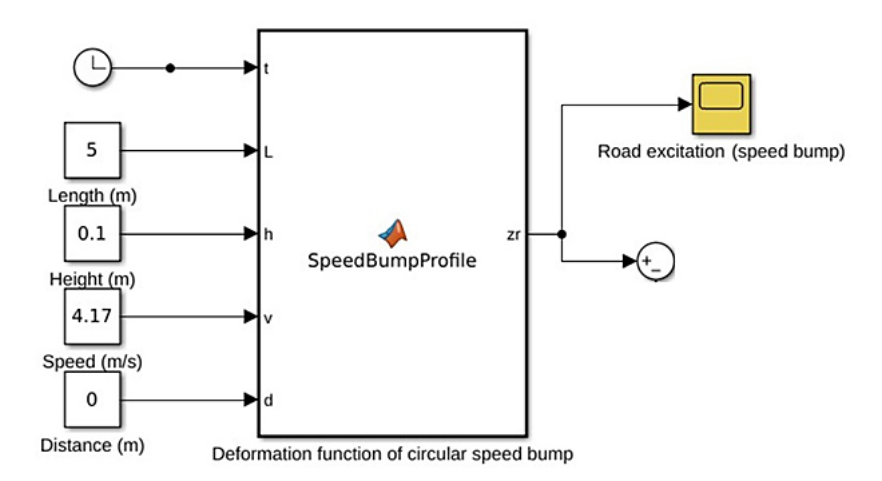


Figure 7. MATLAB function – simulation of excitation by circular speed bump

The profile of the speed bump is modeled using a half-sine wave as input excitation, consistent with approaches adopted in various suspension studies [3]. In this work, we incorporate the geometric standards and technical criteria for speed bumps established by the Ministry of Transport and Communications (MTC) of Peru [9], which define critical parameters such as height, length, and slope based on design speed.

The vertical road displacement  $z_r(t)$  is defined by the following expression:

$$\begin{split} z_r(t) &= 0 \text{ para } t < \frac{d}{v} \text{ } y \text{ } t > \frac{d+L}{v} \\ z_r(t) &= h. \sin \left[ \frac{\pi v}{L} \left( t - \frac{d}{v} \right) \right] \text{ para } \frac{d}{v} < t < \frac{d+L}{v} \end{split} \tag{7}$$

where: h and L represent the height and length of the speed bump, respectively, v is the vehicle's speed. t is the simulation time, which begins when the vehicle approaches within a distance d of the obstacle.

This formulation simulates the vehicle traversing a sinusoidal bump at a constant velocity

of 15 km/h. The function is implemented in a MATLAB Simulink block to generate dynamic excitation (Figure 7), and Table 4 summarizes the different test scenarios used to evaluate the suspension response.

It should be noted that the suspension force  $f_s$  transmitted to the chassis is considered a transient dynamic load, as it appears and disappears within a limited time interval. To perform the transient analysis, a modal analysis is conducted first.

In the case of speed bumps, Table 4 was used to define the input data in Simulink, generating the different excitation curves corresponding to each scenario (Figure 9). The selected dimensions are based on the technical criteria in Table 5 (Figure 8), which links the expected speed with the radius, chord length, and crossing speed, in accordance with road engineering studies aimed at maximizing user safety and comfort. The first three categories of this table were taken, classified as Case 1, Case 2, and Case 3, whose parameters are detailed in Table 6.

<b>Table 4.</b> Simulation conditions: different circular	pothole	profiles and	l vehicle speeds
---	---------	--------------	------------------

	Speed r			
Case	Caso	Altura	Largo	Vehicle speed (km/h)
	(Table 5)	(mm)	(mm)	
1	- 25 km/h			5
2		100	3500	10
3	A			15
1	- 30 km/h			5
2		100	4000	10
3	- В			15
1	- 35 km/h			5
2		100	5000	10
3	- C			15

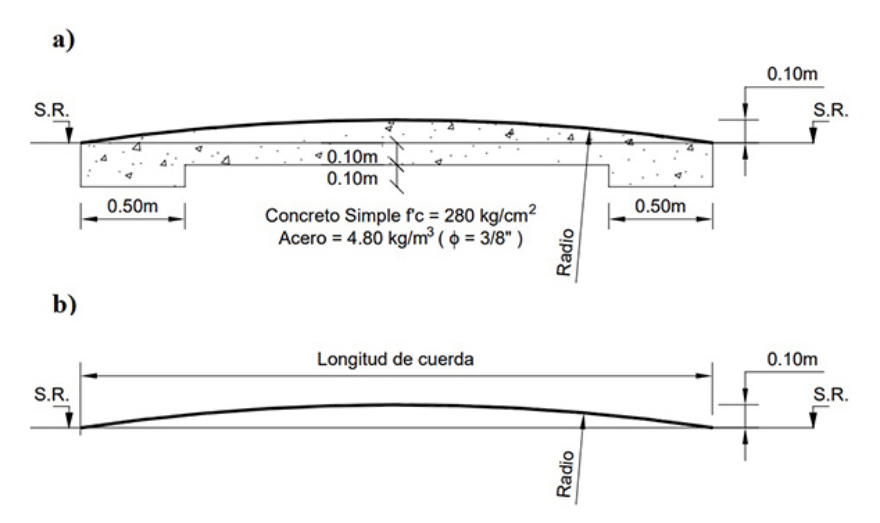


Figure 8. Geometry of circular speed reducers: (a) portland concrete (b) asphalt concrete [9]

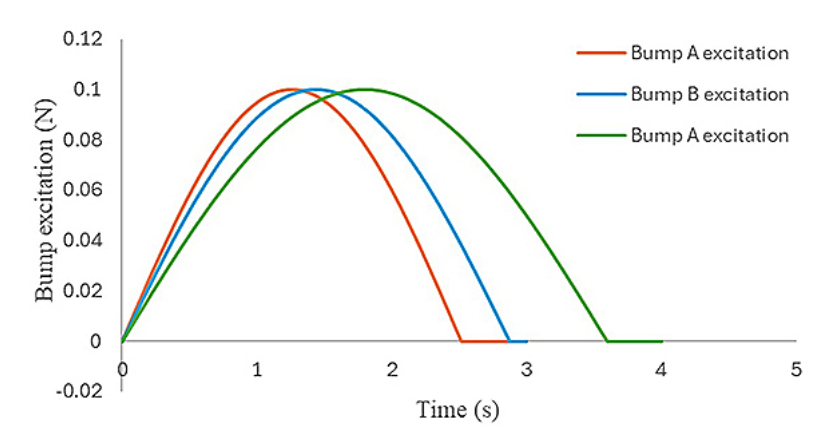


Figure 9. Excitation profiles generated by speed bumps A, B and C

Table 5.	Radii and	l chord	lengths	for	circu	lar-sect	10n
speed bu	mps [9]						

Expected	Radius	Chord	Speed during
speed	(m)	length (m)	passage
(km/h)	. ,	length (III)	(km/h)
25	15	3.5	10
30	20	4.0	15
35	31	5.0	20
40	53	6.5	25
45	80	8.0	30
50	113	9.5	35

To evaluate the structural behavior of the chassis under real operating conditions, static and dynamic load simulations were implemented, adapted to the environmental characteristics and specific design of the cleaning vehicle. In the dynamic analysis, three main scenarios were simulated using forces obtained from the suspension model in Simulink:

 Frontal impact simulation – dynamic loads were simultaneously applied to the front

- wheel support points, representing the impact when passing over a speed bump or pothole. This load case allows analysis of the chassis response to vertical bending stresses.
- Rear impact simulation similar to the previous case, but focusing the response on the rear support points of the chassis.
- Torsional load simulation a dynamic load was applied to a single front support point, simulating one wheel passing over a lateral obstacle. This scenario allows evaluation of the torsional stiffness of the chassis and its ability to resist asymmetric deformations.

Additionally, a static analysis was performed by applying vertical loads to the chassis support points, modeling the total vehicle weight and maximum garbage load. This analysis allows determination of stresses and deformations under permanent load conditions, validating the chassis' ability to withstand continuous operation without compromising its structural integrity. The chassis damping factor was defined as 0.02 [24], a typical value for welded steel structures, assuming that the wheels maintain constant contact with the road in all scenarios.

A 4-second test simulation was performed to determine the maximum suspension force, whether it was in the initial or subsequent reaction phase, using Case A as a test. In this image, we can see that the difference is minimal, so the initial reaction, i.e., the first peak of the suspension, was taken for the following analyses (Figure 10).

#### Suspension force analysis

The dynamic analysis performed with Simulink characterized the forces transmitted to the chassis when overcoming urban obstacles. The results show values ranging from 133 N to 585 N, with significant variations depending on speed and type of obstacle. When tripling the speed from 5 to 15 km/h, the suspension forces

increased between 2.1 and 3.2 times, revealing a nonlinear relationship that justifies speed limits in uneven areas.

The simulations showed that obstacles with a more pronounced profile (type A) generate up to 30% more load than more extensive obstacles (type C) at equal speeds, due to the higher rate of change in suspension deformation. The most critical case occurred when overcoming a type A obstacle at 15 km/h, reaching a maximum force of 585 N in just 0.04 seconds (Figure 11). Although lower than the values recorded for conventional vehicles, these results are consistent with the compact design and diagonal suspension system implemented. The rapid dissipation of energy (characteristic times of less than 0.05 s) confirms the effectiveness of the system for urban operations at controlled speeds. The forces obtained represent only 17% of the material's elasticity limit, which validates the safety margin adopted in the structural design.

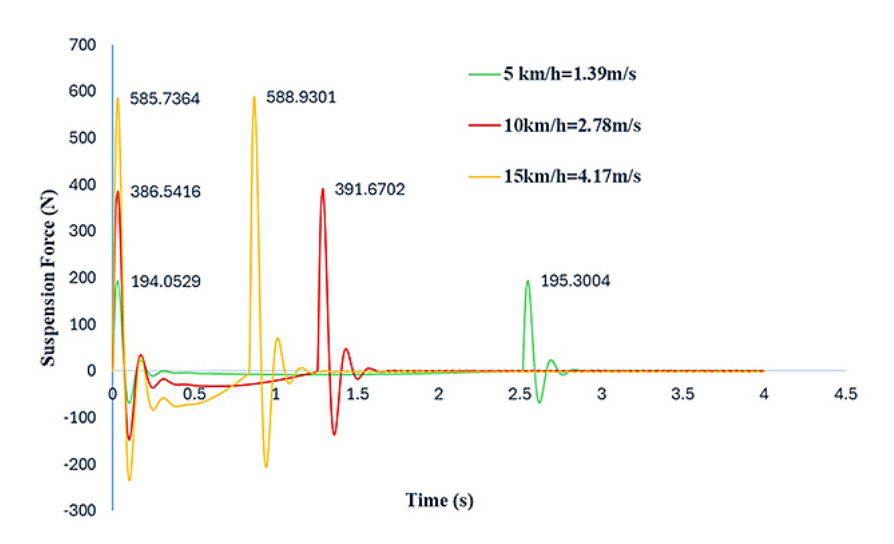
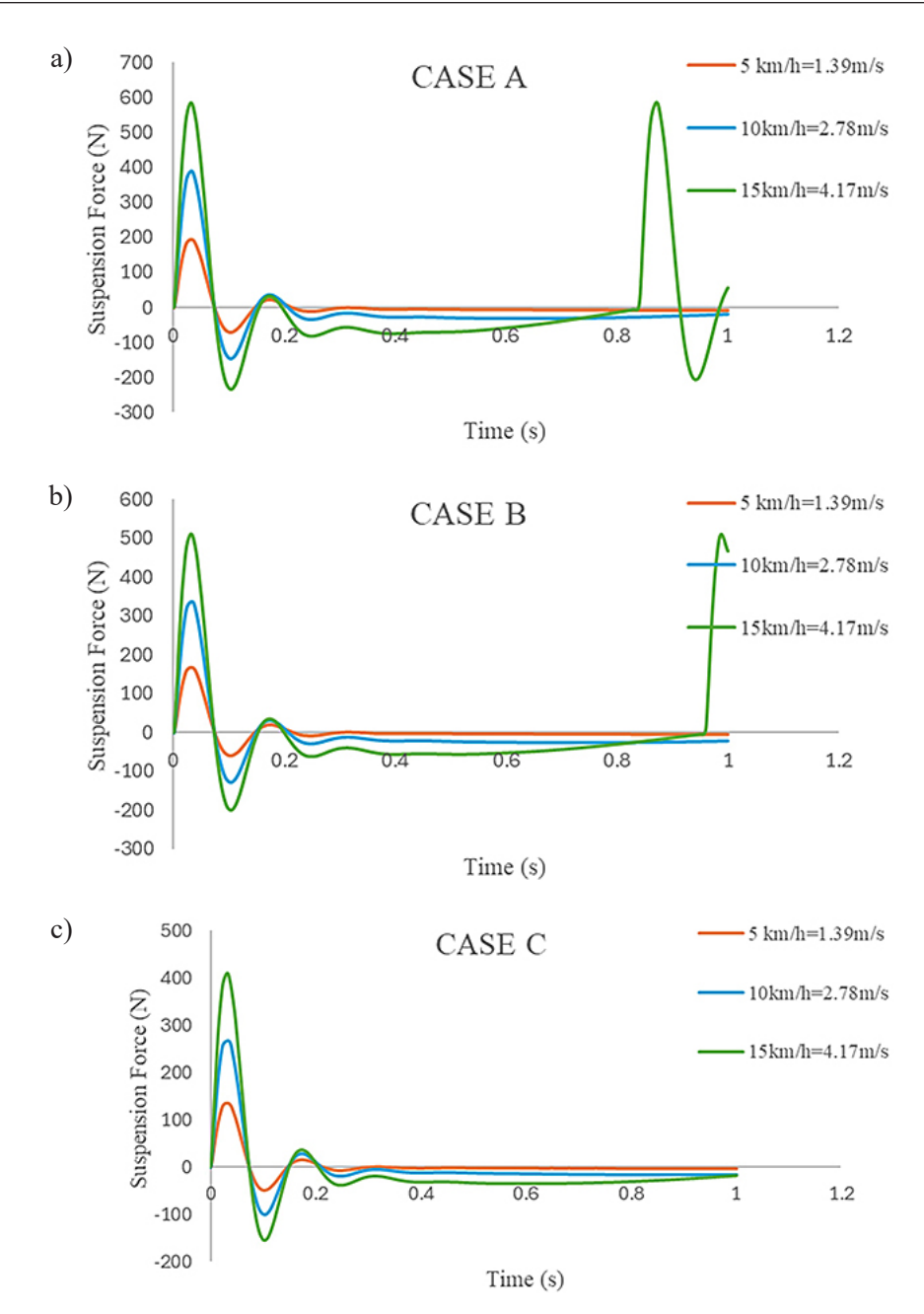


Figure 10. Force-time function for a type A speed bump at 5, 10 and 15 km/h over a 4-second simulation

<b>Table 6.</b> Suspension for	rces results for th	e different cases
--------------------------------	---------------------	-------------------

Case	Category (Table 6)	Cart speed (km/h)	Suspension force (N)
1	"	5	186.05
2	25 km/h	10	369.08
3	A	15	585.04
1	30 km/h B	5	163.22
2		10	323.69
3		15	512
1	0.5.1	5	133.16
2	35 km/h C	10	258.8
3		15	407.87



**Figure 11.** Suspension force-time response at t = 1 s for: a) type I, b) type II, c) type III speed bumps, each tested at 5, 10, and 15 km/h

#### **MODAL ANALYSIS**

The modal analysis excluded the first six rigid-body modes and focused on the next twenty flexible modes, identifying the first three as critical due to their high effective mass participation in the chassis's dynamic response (Table 7).

Mode 1, at a natural frequency of 50.33 Hz, exhibited dominant lateral bending in the X-direction, primarily involving deformation of the side rails. This mode showed the highest effective mass participation of 20.39 %, indicating critical responsiveness to lateral excitation such as

frontal impacts. This frequency lies just above the typical excitation band from terrain irregularities (5–30 Hz), but coupling with higher harmonics justifies its consideration.

Similar lateral bending patterns and their implications for structural response have been observed in modal studies of vehicle body frames under dynamic loading [25].

In the vertical direction (Y), Mode 2 at 57.29 Hz showed an effective mass participation of 16.77%, being responsible for the maximum deformations observed in the roof structure during simulations. Its characteristic vertical bending

**Table 7.** Natural frequencies of the chassis

Mode	Frequency	Modal participation factors		Effective mass			
wode	(Hz)	Factor X	Factor Y	Factor Z	X (%)	Y (%)	Z (%)
1	50.33	0.4516	0.0016	0.0016	20.39	0	0
2	57.29	0.0018	0.4096	0.0182	0	16.77	0.03
3	69.85	0.1712	0.0154	0.0234	2.93	0.02	0.05
4	72.11	0.0033	0.0016	0.2001	0	0	4
5	78.11	0.0097	0.0975	0.3902	0.01	0.95	15.22
6	79.33	0.0093	0.0139	0.0664	0.01	0.02	0.44
7	90.32	0.2818	0.0056	0.0006	7.94	0	0
8	101.56	0.197	0.0446	0.1268	3.88	0.2	1.61
9	101.88	0.0897	0.0879	0.2708	0.8	0.77	7.33
10	105.68	0.0787	0.0076	0.0191	0.62	0.01	0.04
11	133.45	0.0026	0.2622	0.0519	0	6.87	0.27
12	151.76	0.0015	0.0172	0.2644	0	0.03	6.99
13	160.86	0.0098	0.0057	0.0107	0.01	0	0.01
14	174.26	0.001	0.207	0.2476	0	4.29	6.13
15	183.06	0.2316	0.0015	0.0035	5.36	0	0
16	200.51	0.1149	0	0.0205	1.32	0	0.04
17	203.28	0.0223	0.0258	0.0905	0.05	0.07	0.82
18	206.02	0.0161	0.0215	0.0496	0.03	0.05	0.25
19	227.4	0.0623	0.019	0.0017	0.39	0.04	0
20	231.21	0.0138	0.1063	0.011	0.02	1.13	0.01

modal shape explains approximately 78% of the recorded vertical displacements, particularly when traversing extended obstacles like speed bumps. Comparable vertical deformation responses under modal excitation have been analyzed in vehicle hood structures using free-free modal analysis techniques.

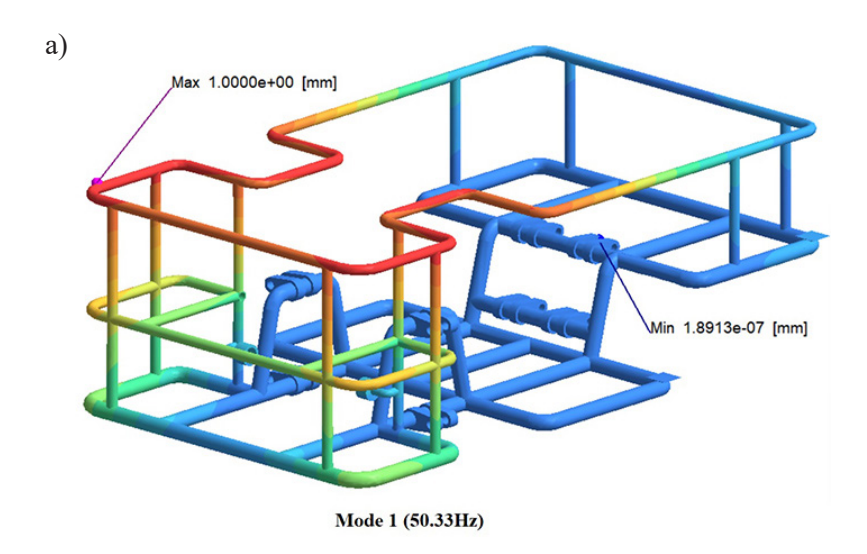
Mode 5 at 78.11 Hz exhibited a characteristic global torsion pattern in the Z-direction, with 15.22% effective mass concentrated mainly in the rear suspension towers. This mode becomes critical for asymmetric loading scenarios, such as when one wheel encounters an obstacle while the others remain on flat ground, generating significant shear stresses at structural joints. This type of global torsion and its dynamic effects are consistent with findings in support frame studies for agricultural vehicles subjected to irregular terrain conditions [26].

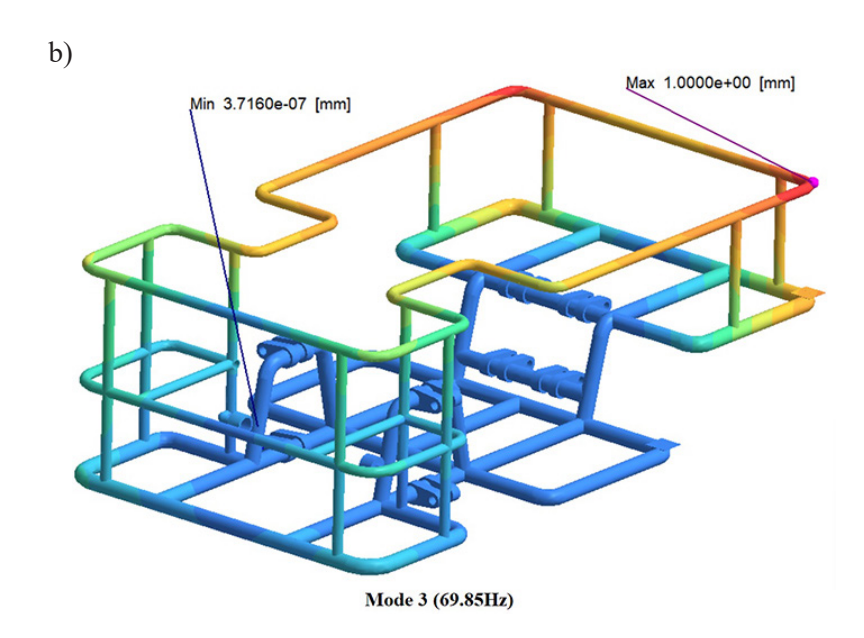
The identified natural frequencies (50–80 Hz) maintain a sufficient safety margin relative to typical excitation sources encountered during operation (5–30 Hz), thereby minimizing the risk of resonance phenomena [27]. Structural responses under these modes suggest that higher stress concentrations occur along the

main longitudinal members and at the shock absorber bases (Figure 12). Numerical simulations also indicated that vertical and torsional deformations are amplified at the roof and rear suspension towers, respectively. When compared to baseline configurations, enhanced models with increased section thicknesses and additional cross-bracing demonstrated a 35–40% reduction in vibration amplitudes, while maintaining safety factors above 1.8 under the most demanding loading cases [28].

### NUMERICAL SIMULATION-BASED DYNAMIC ANALYSIS OF THE CHASSIS

The dynamic analysis of the chassis was conducted using Altair SimSolid, a meshless finite element tool that enables efficient structural evaluation of complex geometries. The dynamic loads were derived from the suspension forces obtained through a mathematical model implemented in MATLAB Simulink, simulating interactions with standardized road humps. The structural assessment was based on the von Mises equivalent stress criterion, which identifies





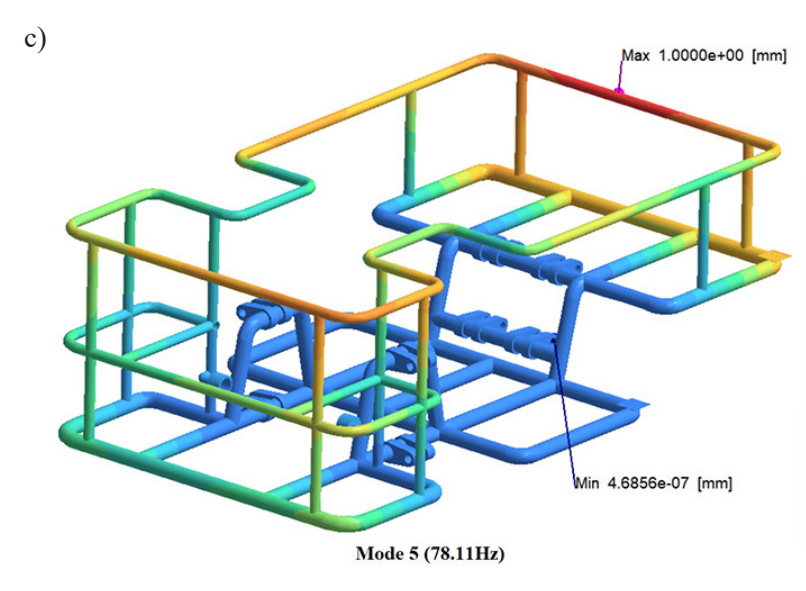


Figure 12. Deformation of critical vibration modes a) Mode 1, b) Mode 3, c) Mode 5

regions susceptible to plastic deformation under multiaxial loading. To verify structural integrity, dynamic safety factors were calculated by comparing the peak stresses with the yield strength of the AISI 1040 steel (353 MPa).

The analysis considered three main load configurations: frontal, rear and torsional, using as input the suspension forces obtained for nine operating cases combining different obstacle profiles (A, B, C) with speeds between 5 and 15 km/h. The critical case corresponded to scenario A3 (type A obstacle at 15 km/h), which generated the maximum suspension force 585.04 N and was used as reference for the other studies. The updated finite element simulation showed that the maximum von Mises stress 5.528 MPa occurred at 0.0131 s, mainly concentrated on the inner curvature of the rear bar supporting the circular brush motor system and its transmission, as well as at the terminals of the front suspension connected to the crossbars. In terms of deformation, the maximum displacement 0.1119 mm was observed at 0.0128 s on the horizontal front roof bar, followed by 0.0915 mm on the lateral roof bars and 0.0508 mm on the rear horizontal bar. The obtained safety factors and dynamic load factor were estimated using dynamic simulation results in MATLAB Simulink.

#### LOADING CONDITIONS ANALYSIS

Stress concentrations were identified in the suspension tower mounts and joint regions of the side rails, while displacement peaks occurred along the upper roof structure and the lateral frames. The equivalent von Mises stress was used to quantify the severity of stress distributions under dynamic conditions. The formulation for von Mises equivalent stress is given by [26]:

$$= \sqrt{\frac{(\sigma_1 + \sigma_2)^2 + (\sigma_2 + \sigma_3)^2 + (\sigma_1 + \sigma_3)^2}{2}}$$
(8)

According to the von Mises failure criterion, a material starts to yield when the equivalent stress reaches the material's yield strength, which can be mathematically represented as:

$$\sigma_{VonMises} \ge \sigma_{limit}$$
 (9)

The creep strength is commonly used as the default criterion for evaluating structural safety;

however, the software also allows the selection of ultimate tensile strength or a custom-defined limit based on user specifications. The factor of safety (FOS) is calculated as:

$$factor of safety(FOS) = = \frac{\sigma_{limit}}{\sigma_{VonMises}}$$
(10)

In scenarios involving pure shear stress, where only  $\sigma_{12} = \sigma_{21} \neq 0$ , and all other stress components are zero, the von Mises criterion simplifies to the following expression for critical shear stress:

$$\sigma_{12}m\acute{a}x = \frac{\sigma_{yield}}{\sqrt{3}} =$$

$$= 0.5777(\sigma_{yield})$$
(11)

In the rear load case, the maximum von Mises stress was 5.528 MPa at 0.0131 s (Figure 13), localized in a small region at the inner curvature of the rear bar and at the suspension terminals. The structure maintained a safety factor of 63.9, well within elastic limits. The peak displacement was 0.119 mm at the roof bar (Figure 14).

### Torsional load analysis and static-dynamic comparison

The torsional load analysis confirmed asymmetric behavior between the left and right sides of the chassis. Under this condition, the maximum von Mises stress reached 5.528 MPa at 0.0131 s, concentrated on the internal curvature of the rear bar and the front suspension terminals. The maximum displacement was 0.1119 mm, located on the front left section of the roof. All stress levels remained well within the elastic range of AISI 1040, with a minimum dynamic safety factor of 63.9, confirming the structural integrity of the chassis under asymmetric torsional excitation and highlighting the localized sensitivity of specific zones.

#### Comparative static analysis

Under static loading, the chassis experienced a maximum von Mises stress of 1.68 MPa and a maximum displacement of 0.21 mm. In contrast, transient dynamic analysis revealed higher stress values (5.528 MPa) but lower peak displacements (0.119 mm), due to inertia redistribution and structural vibration. These differences highlight the importance of combining both static and dynamic simulations to ensure mechanical integrity under real operating conditions.

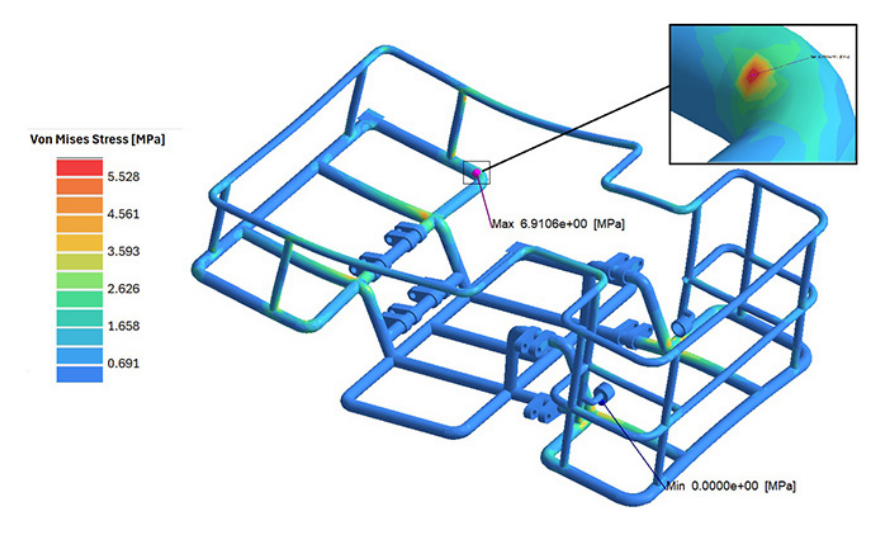


Figure 13. Results of stress distribution at 0.0131 s for Case 3

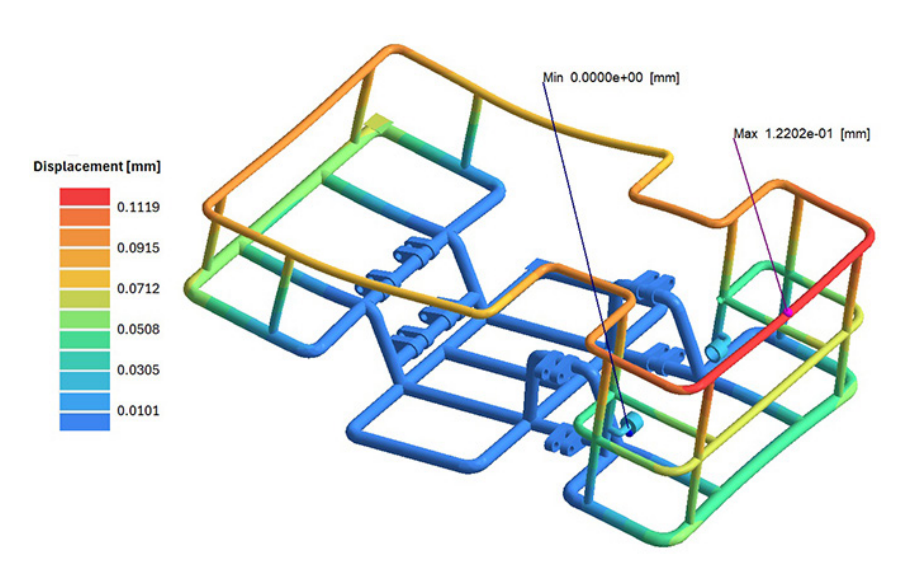


Figure 14. Displacement results for transient dynamics link to modal

#### **Dynamic load factor**

The comparison between static and dynamic analyses yielded a dynamic load factor of 3.29, indicating that operational stresses can increase more than threefold during transient loading events. This value is within the expected range for vertical impacts in light electric vehicles and confirms the importance of incorporating dynamic analyses in the design process. Deviations from theoretical 4g benchmarks may be attributed to the specific geometry of the obstacles, the use of a diagonal suspension system, and the quartervehicle modeling approach with a suspended mass of 50 kg. The computed safety factors 5.19 under static conditions and 1.94 under dynamic loads demonstrate that the chassis remains within the elastic limit of the selected AISI 1040 steel

throughout all evaluated scenarios. These results emphasize the relevance of accounting for load amplification when assessing structural reliability under irregular urban driving conditions, particularly in critical areas such as suspension towers and roof joints.

### **CHASSIS DYNAMIC ANALYSIS RESULTS**

The structural response of the chassis under dynamic loading conditions was evaluated using Altair SimSolid, which enabled an efficient meshless finite element analysis of the complex geometry. Dynamic loads were obtained from a quartercar model implemented in MATLAB Simulink, simulating the interaction between the chassis and standardized road obstacles (categories A, B, and C) at various speeds ranging from 5 to 15 km/h. A total of nine operating cases were analyzed, as summarized in Table 6. Among them, the most critical condition corresponded to case A3 (type A obstacle at 15 km/h), which produced the maximum suspension force of 585.04N. This load case was selected for the transient structural analysis to capture the peak dynamic response of the chassis.

The maximum von Mises stress reached 5.528 MPa at 0.0131 seconds and was primarily concentrated on the inner curvature of the rear structural bar that supports the circular brush motor and transmission system, as well as at the mounting terminals of the front suspension, where it connects to the crossbars. Regarding deformation, the maximum displacement was recorded as 0.1119 mm at 0.0128 seconds, located on the horizontal front roof bar. Additional deformations were observed on the lateral roof bars (0.0915 mm) and the rear horizontal bar (0.0508 mm).

The results were evaluated against the yield strength of AISI 1040 steel (353 MPa), with all observed stresses remaining well within the elastic limit. Consequently, the calculated dynamic safety factors confirmed that the structure can withstand the simulated operating conditions without undergoing plastic deformation. These findings validate the robustness of the chassis design for urban service vehicles traversing irregular road profiles at low to moderate speeds.

#### **CONCLUSIONS**

The dynamic structural analysis of the chassis for the unmanned electric sweeper vehicle demonstrated that the proposed design is mechanically robust under realistic operating conditions, thereby validating the initial objectives of this research. The hybrid methodology, which integrates a quarter-car dynamic model in MATLAB/Simulink with Altair SimSolid's meshless finite element analysis, was confirmed as an efficient and precise approach for evaluating the structural integrity of lightweight vehicles. The main scientific findings of this study are:

1. Quantification of dynamic stress amplification: We determined that impact forces on the chassis are significantly greater than static forces, with a dynamic load factor of 3.29. This result validates the need to move beyond static analysis and highlights that operational

- stresses can more than triple in irregular urban environments.
- 2. Validation of the diagonal suspension design: The use of a geometric correction function in the simulation model not only allowed for a precise representation of the diagonal suspension's response but also demonstrated its effectiveness in dissipating force peaks of up to 585 N. This design and its rigorous modeling ensure that the structure can withstand highmagnitude impacts, protecting internal systems and guaranteeing vehicle longevity.
- 3. Confirmation of structural integrity and material suitability: The most critical load case generated a maximum von Mises stress of 5.528 MPa, which is far below the yield strength of AISI 1040 steel (353 MPa). The calculated safety factors (a minimum of 1.94 under dynamic load) and identified natural frequencies (well clear of the terrain's excitation range) confirm the material's suitability and the structural viability of the chassis for operation in Arequipa's topography.

This study not only fulfills the objective of validating the robustness of the proposed design but also establishes a reproducible methodological framework that contributes to the body of knowledge on lightweight autonomous vehicle design, demonstrating that integrating system dynamics with advanced structural analysis is crucial for ensuring safety and durability in demanding operational environments.

#### **Acknoledgements**

We thank the Universidad Nacional de San Agustín de Arequipa for their support and knowledge, and NovaLabs for the resources and supervision provided.

#### **REFERENCES**

- Jeyapandiarajan P, Kalaiarassan G, Joel J, Shirbhate R, Felix Telare F, Bhagat A. Design and Analysis of Chassis for an Electric Motorcycle. Mater Today Proc [Internet]. 2018 Jan 1 [cited 2025 Jul 24];5(5):13563-73. Available from: https://www.sciencedirect.com/science/article/abs/pii/S2214785318305558
- 2. Wang S, Wang D. Crashworthiness-based multiobjective integrated optimization of electric vehicle chassis frame. Archives of Civil and Mechanical

- Engineering [Internet]. 2021;21(3):103. Available from: https://doi.org/10.1007/s43452-021-00242-2
- 3. Kulkarni A, Ranjha SA, Kapoor A. A quarter-car suspension model for dynamic evaluations of an in-wheel electric vehicle. Proceedings of the Institution of Mechanical Engineers, Part D: Journal of Automobile Engineering [Internet]. 2018;232(9):1139–48. Available from: https://doi.org/10.1177/0954407017727165
- Gaikwad A, Chavan U. AISI 4130 and E250BR alloy steels chassis structural analysis and performance comparison. Mater Today Proc [Internet]. 2023 Jul 1 [cited 2025 Jul 24]; Available from: https://www.sciencedirect.com/science/article/abs/pii/S2214785323036623?casa\_token=1Ook4eZL\_aYAAAAA:k6cgQ4iBL\_G6JDqhan\_oQSJbRRvBH6HX5q-mSo\_2uaalQoxaJsAAlGKP4eoOrqiPGxBLl1Az1Bc
- 5. Logan DL. A first course in the finite element method. Thomson; 2007.
- Zamzam O, Ramzy AA, Abdelaziz M, Elnady T, El-Wahab AAA. Structural performance evaluation of electric vehicle chassis under static and dynamic loads. Sci Rep [Internet]. 2025;15(1):5168. Available from: https://doi.org/10.1038/s41598-025-86924-w
- Park DW, Papagiannakis AT, Kim IT. Analysis of dynamic vehicle loads using vehicle pavement interaction model. KSCE Journal of Civil Engineering [Internet]. 2014 Nov 1 [cited 2025 Jul 24];18(7):2085–92. Available from: https://www.sciencedirect.com/science/article/pii/S1226798824006251
- 8. Gupta G, Tyagi RK, Rajput SK, Saxena P, Vashisth A, Mehndiratta S. PVD based thin film deposition methods and characterization / property of different compositional coatings A critical analysis. Mater Today Proc [Internet]. 2021 Jan 1 [cited 2025 Jul 24];38:259–64. Available from: https://www.sciencedirect.com/science/article/abs/pii/S2214785320352238?casa\_token=-kfMyB5twO-kAAAAA:-\_A0db73zrGRIba\_S1b7a9k0U5E-9yhfXDF7mruQG6Up33MOvzKIQcXB-Qau-4MoaAwSYcFZrKccU
- Ministerio de Transportes y Comunicaciones del Perú. 06\_Reductores de Velocidad [Internet]. [cited 2025 Jul 24]. Available from: https://portal.mtc. gob.pe/transportes/caminos/normas\_carreteras/ MTC%20NORMAS/ARCH\_PDF/06\_Reductores%20de%20Velocidad.pdf
- 10. Lak MA, Degrande G, Lombaert G. The effect of road unevenness on the dynamic vehicle response and ground-borne vibrations due to road traffic. Soil Dynamics and Earthquake Engineering [Internet]. 2011 Oct 1 [cited 2025 Jul 24];31(10):1357–77. Available from: https://www.sciencedirect.com/science/article/abs/pii/S0267726111001564?via%3Dihub
- 11. Jamali MS, Ismail KA, Taha Z, Aiman MF.

- Development of Matlab Simulink model for dynamics analysis of passive suspension system for lightweight vehicle. In: Journal of Physics: Conference Series. Institute of Physics Publishing; 2017.
- 12. Apanovitch -Simsolid V. Using Altair Simsolidtm technology overview.
- 13. Bouafia F, Boualem S, Amin MM El, Benali B. 3-D finite element analysis of stress concentration factor in spot-welded joints of steel: The effect of process-induced porosity. Comput Mater Sci [Internet]. 2011 Feb 1 [cited 2025 Jul 24];50(4):1450–9. Available from: https://www.sciencedirect.com/science/article/abs/pii/S0927025610006555
- 14. Randić M, Pavletić D, Fabić M. Evaluation of the stress concentration factor in butt welded joints: A comparative study. Metals (Basel). 2021 Mar 1;11(3):1–10.
- 15. Sabarivasan V, Sivaraj P, Balasubramanian V, Malarvizhi S. Analysis of failure modes of resistance spot welded dissimilar thickness DP800/AISI 1040 steel joints: An effect of welding current. Journal of Failure Analysis and Prevention [Internet]. 2025;25(1):402–12. Available from: https://doi.org/10.1007/s11668-025-02116-8
- 16. Goher KM, Chenhui K, Fadlallah SO, Shabibi AM Al, Rawahi NZ Al. Transient dynamic impact suppression of a Baja chassis using frontal and rear shock absorbers. International Journal of Crashworthiness [Internet]. 2017 Nov 2;22(6):676–88. Available from: https://doi.org/10.1080/13588265.2017.1301081
- 17. Sharma SK, Lee J, Jang HL. Mathematical modeling and simulation of suspended equipment impact on car body modes. Machines. 2022 Mar 1;10(3).
- 18. Sinclair GB, Beisheim JR, Kardak AA. On the detection of stress singularities in finite element analysis. J Appl Mech [Internet]. 2018 Dec 3;86(2). Available from: https://doi.org/10.1115/1.4041766
- 19. Pang L, Lin G, Hu Z. A refined global-local approach for evaluation of singular stress field based on scaled boundary finite element method. Acta Mechanica Solida Sinica [Internet]. 2017 Apr 1 [cited 2025 Jul 24];30(2):123–36. Available from: https://www.sciencedirect.com/science/article/abs/pii/S0894916617300939?casa\_token=kwqtKvL-XfNgAAAA:DdLpMaMSnawzLGhB1HAfxk11 6Q6ymHuiLQ4EE7AiNyp5W6uNhybIBmgKg0x-bnW5Mpd42XPRwZU4
- 20. Bulling J, Gravenkamp H, Birk C. A high-order finite element technique with automatic treatment of stress singularities by semi-analytical enrichment. Comput Methods Appl Mech Eng [Internet]. 2019 Oct 1 [cited 2025 Jul 24];355:135–56. Available from: https://www.sciencedirect.com/science/article/abs/ pii/S0045782519303688?utm\_source=chatgpt.com
- 21. Gatti G, Svelto C. Exploiting nonlinearity for the

- design of linear oscillators: Application to an inherently strong nonlinear X-shaped-spring suspension. Mech Syst Signal Process [Internet]. 2023 Aug 15 [cited 2025 Jul 24];197:110362. Available from: https://www.sciencedirect.com/science/article/pii/S0888327023002698
- 22. Tien NN, Van HN, Duy VN, Trinh HP. Simulation-based comparative analysis of different chassis configurations of hybrid fuel cell vehicle. International Journal of Thermofluids [Internet]. 2024 Nov 1 [cited 2025 Jul 24];24:100968. Available from: https://www.sciencedirect.com/science/article/pii/S2666202724004087
- 23. Panananda N, Daowiangkan S, Intaphrom N, Kantapam W. Influence of shock absorber installation angle to automotive vehicle response. Journal of Research and Applications in Mechanical Engineering. 2017;5(2).
- 24. Kudu FN, Uçak Ş, Osmancikli G, Türker T, Bayraktar A. Estimation of damping ratios of steel structures by Operational Modal Analysis method. J Constr Steel Res [Internet]. 2015 Sep 1 [cited]

- 2025 Jul 24];112:61–8. Available from: https://www.sciencedirect.com/science/article/abs/pii/S0143974X15001339?via%3Dihub
- 25. Subramanyam B, Rao N, Prakash RL, Rajavardhan DSK, Sankarudu BSK, Ganesh P. Modal Analysis On Go-Kart Chassis. Int J Eng Adv Technol [Internet]. 2019; Available from: www.ijeat.org
- 26. Macedo J, Molina J, Silva Vidal Y, Mendoza A, Canazas J, Diaz C. Static analysis and topological optimization of photovoltaic panel support using recycled polymeric plastic. Advances in Science and Technology Research Journal [Internet]. 2025;19(6):167–80. Available from: https://doi. org/10.12913/22998624/203079
- 27. Han X, Chi X. Modal analysis and structural noise control of vehicle body frame. In: Vibroengineering Procedia. EXTRICA; 2024,135–41.
- 28. Pinzaru V, Bujoreanu C, Barat O. Structural damping analysis of a vehicle front hood: Experimental modal parameters extraction and simulation correlation. Machines. 2024 Dec 1;12(12).